Electrochimica Acta 421 (2022) 140493

Contents lists available at ScienceDirect

Electrochimica Acta

journal homepage: www.journals.elsevier.com/electrochimica-acta

Effect of sodium addition on lattice structure and tuning performance in sodium rich $Na_xTm_{2-x}O_2$ type cathode materials (Tm=Mn and Cr; X=1.05–1.3) - a study

Bala Krishnan Ganesan [a,1], Ui Rim Son [a,1], Ranjith Thangavel [b], Yun-Sung Lee [a,*]

[a] School of Chemical Engineering, Chonnam National University, Gwangju 61186, South Korea
[b] School of Energy Science and Engineering, Indian Institute of Technology Guwahati, Guwahati 781039, India

ARTICLE INFO

Keywords:
Sodium rich cathode
Sodium ion battery
Rietveld analysis
Electron density mapping

ABSTRACT

Na-rich transition metal oxides are promising cathode materials owing to their high theoretical capacity and ability to be used in a solid-state sodium battery. However, one of their drawbacks is that they are prone to capacity loss. The reduction in capacity during cycling is attributed to oxygen loss, resulting in rapid capacity fading. To address this issue, a $Na_xTm_{2-x}O_2$ type cathode material (Tm = Mn and Cr; X = 1.05–1.3) was synthesized successfully and analyzed for desired cathode attributes. The material was synthesized using the solid state method and quenching to achieve a crystalline cathode structure. Different sodium stoichiometries were used and electrochemically tested. The resultant was a $Na_{1.1}Cr_{0.9}O_2$ electrode that achieved a high capacity of 110 mAh/g at 1000 mA/g compared with other compositions. The superior performance of $Na_{1.1}Cr_{0.9}O_2$ over other Na-rich stoichiometries (1.05–1.3) with Mn as the transition metal was analyzed using X-ray characterization techniques and other electrochemical techniques. This high-capacity cathode was used to construct a full cell battery by coupling with a hard-carbon anode to demonstrate its applicability in the real world. The constructed battery with a $Na_{1.1}Cr_{0.9}O_2$ cathode exhibited a high capacity with a high energy density of 223 Wh/kg and power density of 1100 kW/kg.

1. Introduction

The number of inventions and developments in the last century has been higher than those in the previous centuries cumulatively. The harnessing of electricity can be considered as a key invention that opened a new direction and paved the way for many other inventions. Owing to a rapidly developing human society, the demand for energy and its storage is rising substantially. Although in the past decades, energy was produced by burning fossil fuels, the paradigm has recently shifted towards more eco-friendly sources such as wind, solar, and nuclear power. However, in most cases, the production methods for these types of energy are inconsistent and highly dependent on various external factors such as battery and supercapacitor quality. For large-scale energy storage, lithium-ion battery technology is commonly used. However, sodium ion batteries (SIBs) have recently gained more attention as a potential replacement for lithium-ion batteries owing to the availability of sodium and equal distribution of the element around the world [1–3].

Compared with lithium batteries, the cathode material options for SIBs are very few owing to the small number of research groups focusing on SIBs and larger sodium ion exposing cyclability difficulties [4]. Most of these cathode materials can be classified as either sodium deficient (i.e., Na < 1.0) [5,6] or sodium-rich cathodes (i.e., Na > 1.0) [7–9]. The sodium-deficient type became the more popular subject for research because of its similar structure and properties to its lithium counterpart. Among sodium deficient cathode, in addition to O-type (octahedral) materials, various P-type (prismatic) can occur, giving rise to O3-, P2-, and P3-type cathodes owing to a bigger sodium-ion size [8,10–12]. P2 and O3 are the most widely studied types owing to their superior conductivity and greater stability; however, they lack storage capacity. The P2 type's lack of storage capacity is mainly owing to its lower Na content, whereas the O3 type lacks in structural integrity, resulting in poor cycle stability. Typically, the structural integrity of the P2 type is well-preserved during the sodium extraction process, leading to a more open framework and a direct sodium diffusion process. However in O3 type, the formation of the P3 phase from the O3 phase due to TmO_2 layer

* Corresponding author.
[1] These authors contributed equally to this work.

https://doi.org/10.1016/j.electacta.2022.140493
Received 18 March 2022; Received in revised form 21 April 2022; Accepted 1 May 2022
Available online 3 May 2022

gliding results in capacity loss during cycling [13]. The transition metals used in the TmO_2 layer [14], such as Cr in Na_xCrO_2 [15], V in Na_xVO_2 [16], and Co in Na_xCoO_2 [17], are commonly limited by their capacity and poor rate capability.

In the context of sodium-rich cathode materials, Prussian blue type (PB type) cathodes have been investigated, mostly owing to their advantages such as high theoretical capacity, 3-D open framework, and two-electron redox capability [18–24]. However, because of the extraction of two Na^+ ions, PB type cathodes are vulnerable to structural instability and often results in poor cycle stability. Hence in most cases, the number of usable cycles reported for PB-type materials is insufficient for practical use. By contrast, another type Na-rich i.e. Na-rich layered oxides ($1.0 < Na < 1.4$) are highly stable but lack in theoretical capacity owing to their one-electron redox process and electrical conductivity in some cases [7,25–28]. Additionally, in sodium-rich cathodes, the O^{2-} anions take part in redox reactions, resulting in increased capacity. To break this poor conductivity issue and enhance electrochemical properties, transition metals are often substituted or doped.

Modifying the Li/Na content in layered structure materials can effectively alter the coordination around oxygen atoms, potentially resulting in improved redox kinetics during cycling. Although these improved redox kinetics have been achieved in P-type Na-deficient materials, this has not been realized for Na-rich materials with various Na stoichiometries. In the case of doping or substitution, increasing the Li/Na content can result in extra channels or pathways for Li/Na transportation, thus improving intercalation behavior in Li/Na-rich materials. This was demonstrated by Lun et al. [29,30]. Additionally, Zhao et al. suggested that the interlayer distance between the sodium metal layer, $d_{(O—Na\text{-}O)}$, and transition metal layer, $d_{(O\text{-}Tm\text{-}O)}$, in layered cathodes can affect various properties. In particular, the interlayer distance largely affects the electron distribution and localization around stacking layers, both of which have been relatively unexplored thus far.

Because of the lack of knowledge regarding any intermediates between sodium-deficient layered structures and sodium-rich Prussian pigment structures, Na-rich layered structure is unexplored and expected to exhibit structures with the advantages of both systems, having the appropriate structural integrity and high storage capacity. To achieve this, two of the most investigated layered oxide cathodes, $Na_xTm_{2-x}O_2$-type cathode material with TM=Mn and Cr, were considered, and the Na content was gradually increased from $X = 1.05$ to 1.3. The variation in the storage capacity with respect to the changes in structure (esp. crystal unit cell) and the subsequent changes in electron distribution were analyzed systematically. As the electron distribution of any material is highly associated with their performance or stability, this characteristic must be comprehensively examined [31,32]. Unlike doping or substitutions, which may not result in equal distributions throughout the system, the modification of the structure by increasing the sodium content may be more rational approach for tuning performance. To the best of our knowledge, no investigation has been conducted on these Na-rich stoichiometries, especially for materials using Mn and Cr as transition metals.

2. Experimental section

2.1. Materials synthesis

2.1.1. Synthesis of $Na_xMn_{2-x}O_2$ (NMO)

NMO was synthesized using a conventional solid-state method. Stoichiometric amounts of Na_2CO_3 (Sigma Aldrich, > 99.5%), Manganese (III) oxide (Sigma Aldrich, 99%), and 20 wt% citric acid (Sigma Aldrich, 99%) were grounded for 15 min using a mortar and pestle. The resultant powder was pressed into pellets, heated to 700 °C for 12 h at a heating rate of 5 °C min^{-1} in a muffle furnace, and quenched to room temperature (25 ℃) under full vacuum in a glovebox's chamber to yield NMO. To avoid contact with air and moisture, the samples were stored inside the glovebox for future use.

2.1.2. Synthesis of $Na_xCr_{2-x}O_2$ (NCO)

The same procedure was repeated to obtain NCO, which was synthesized using a conventional solid-state method. Stoichiometric amounts of Na_2CO_3 (Sigma Aldrich, > 99%), Chromia (Sigma Aldrich, 99%) and 30 wt% citric acid (Sigma Aldrich, 99%) were grounded for 15 min using a mortar and pestle. The resultant powder was pressed into pellets, heated to 900 °C for 5 h at a heating rate of 5 °C min^{-1} in a tubular furnace. The samples were taken out at 100 °C and cooled to room temperature (25 ℃) under full vacuum in a glovebox's chamber to yield NCO. To avoid contact with air and moisture, the samples were stored inside the glovebox for future use.

2.2. Material characterization

Crystal structures were characterized by X-ray diffraction (XRD; Cu Ka radiation, Rint 1000, Rigaku, Japan) in a 2q range of 5°–90° The particle morphology, elemental composition, and internal structure were evaluated using field emission scanning electron microscopy (FE-SEM, S-4700, Hitachi, Japan) coupled with an energy-dispersive X-ray spectroscopy (EDX) module and high-resolution transmission electron microscopy (HR-TEM; JEM-2000, EX-II, JEOL, Japan).

2.3. Electrochemical measurements

The electrochemical studies of all samples were performed using CR2032 coin cells assembled inside a glovebox under a controlled atmosphere of ultrapure argon. The cells consisted of the synthesized material as the cathode and metallic Na as the anode separated by a polypropylene separator, with 1 M NaClO4 in a mixture of ethylene carbonate (EC) and diethyl carbonate (DEC) (1: 1, v/v) as the electrolyte. The anode materials were prepared by mixing 2.5 mg of active material with 0.5 mg of Ketjen black and 0.5 mg of teflonized acetylene black (Table 2). The obtained mixtures were pressed on a stainless steel current collector and dried in an oven at 160 °C for 4 h before cell fabrication. Charge–discharge (C–DC) studies were performed for different voltage ranges at current rates varying from 0.1 to 2 A/g using an Arbin BT-2000 battery test system. Cyclic voltammetry and EIS analyses were conducted using an electrochemical analyser (SP-150, Biologic, France).

3. Result and discussions

3.1. X-ray diffraction analysis (XRD)

Initial XRD analysis of NMO-type material reveals the formation of ordered crystalline structure. Upon increasing the sodium stoichiometry from 1.05 to 1.3, the structural integrity collapses, which is clearly shown in Fig. 1. All the phases and peaks are in accordance with card number ICSD 98-002-1028 with a 2θ high intensity peak at 42.6° corresponding to the (111) plane in monoclinic crystal structure and c12/m1 space group. The high intensity peak for Na = 1.05, 1.1 corresponds with the highly crystalline nature of the samples prepared. Upon increasing the Na content from 1.05 to 1.3, the crystallinity is drastically affected as evident from its low intensity peaks. Furthermore, no additional peaks are observed, indicating that no new phases are formed but rather the existing layered structure has collapsed to the spinel structure of $Na_{1.33}Mn_{0.67}O_2$ (or Na_2MnO_3) [33]. The NMO crystal structure with alternating layers of Na and Mn forms a monoclinic structure. With an increase in Na content, the change in lattice parameter could be analyzed by Rietveld analysis. After the increase in Na content, the change in lattice parameter value results in the collapse of the crystal structure due to a significantly larger Na^+ ionic radius (1.0 Å) compared to that of the Mn^{4+} ions (0.58 Å) being substituted. NCO materials also have a crystalline ordered structure. However, unlike in the previous case, with an increase in Na content, its structural integrity is not affected nearly as much, which is made clear through XRD analysis. All

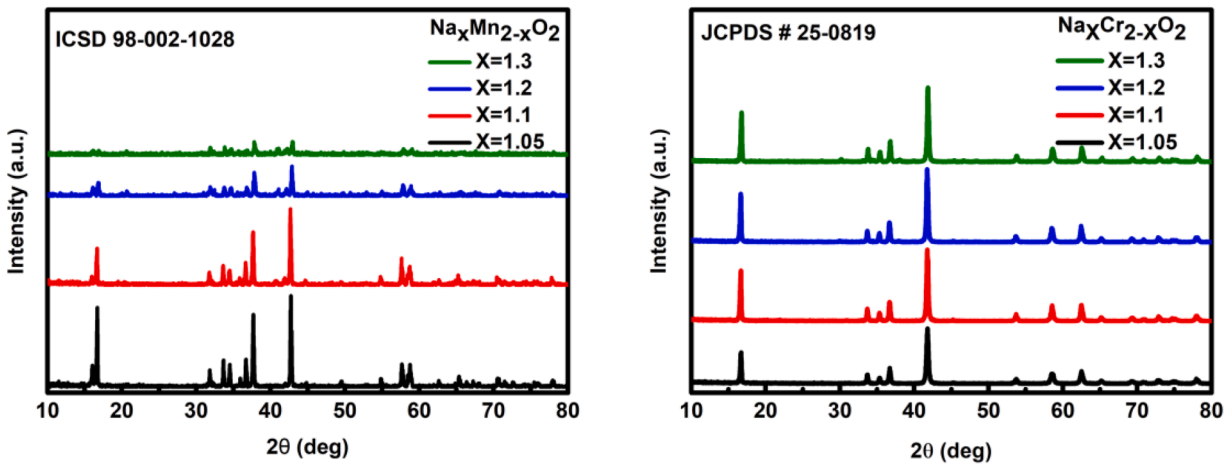

Fig. 1. XRD images of Na-rich NMO materials (left) and NCO materials (right).

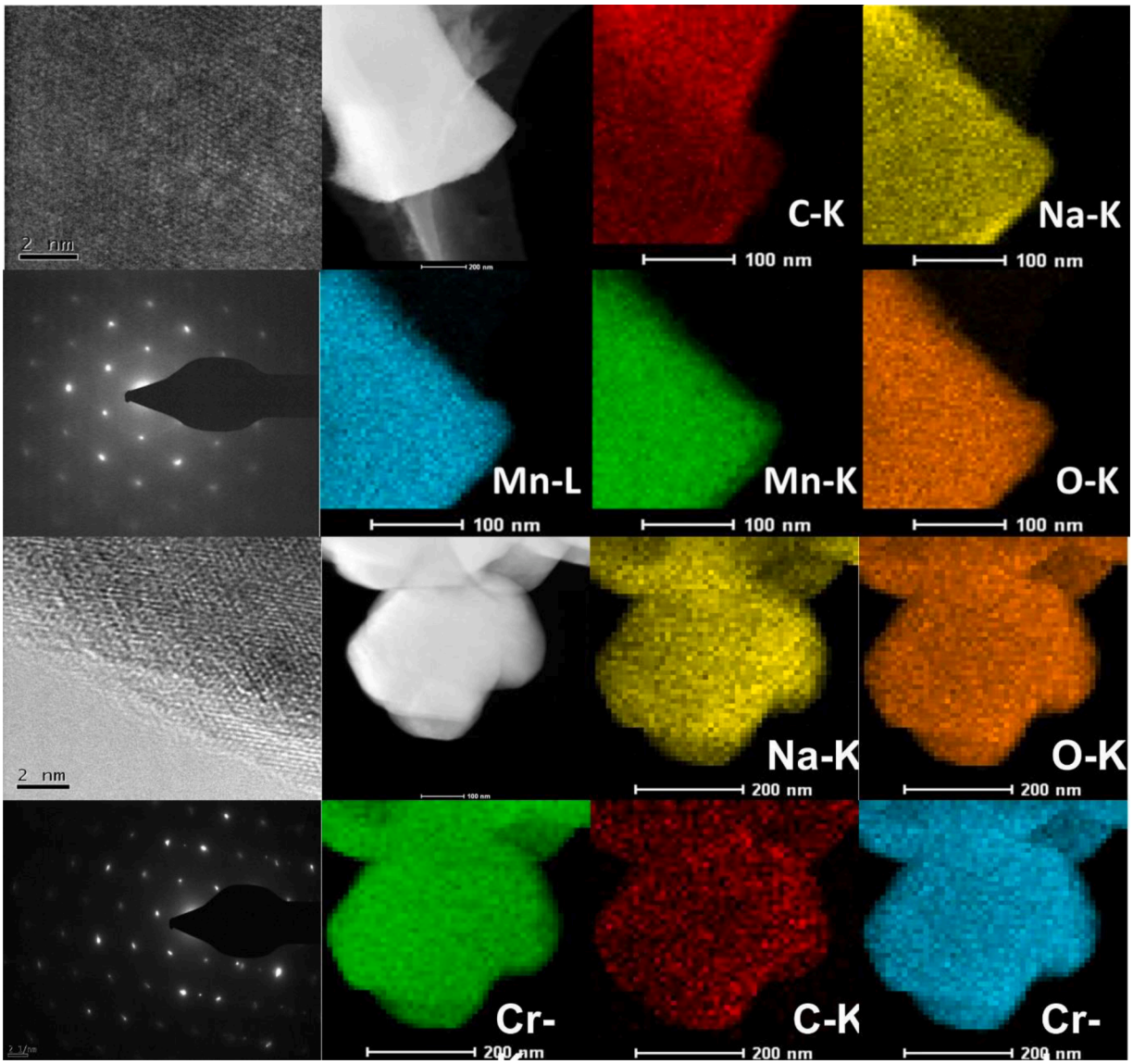

Fig. 2. HRTEM images displaying lattice fringes along with STEM-HAADF images; SAED pattern of NMO materials (top) and NCO materials (bottom).

peaks and phases are in accordance with JCPDS card number 25-0819 with a 2θ high intensity peak at 41.7° corresponding to the (104) plane with a rhombohedral structure and the R3m space group. Throughout the increases in Na content, neither the peak sharpness is affected, nor are there any new peaks that are observed due to extended valence states of +5 availability in Cr. To validate the same, in Fig. S-11 XPS analysis was done on all 4 samples of NCO. It was analysed that binding energy of peaks $2p_{3/2}$ was consistently increasing from 575.7 eV to 576.3 eV due to increase in valence state of Cr from 3+ to beyond 3+. It is interesting that even though Cr (atomic number 24) and Mn (atomic number 25) are so similar in atomic composition, their response to an increase in Na content to their layered oxide electrodes are drastically different.

3.2. Electron microscopy analysis (FE-SEM and HR-TEM)

All of the samples analyzed using FE-SEM showed similar morphology irrespective of TM used and Na content increase. The $Na_{1.1}Mn_{0.9}O_2$ sample consisted of large aggregated secondary particles and had a high crystallinity that was affected by an increase in Na content. On the other hand, for the $Na_{1.1}Cr_{0.9}O_2$ sample, using Cr as TM, the samples retained a high crystallinity irrespective of an increase in Na content. To further investigate the changes in crystal structure, the NCO and NMO samples were analyzed using HR-TEM as shown in Fig. 2. The interplanar spacing of 0.253 nm and 0.236 nm were measured for the (110) and (20$\bar{2}$) planes in NMO samples, which were in perfect agreement with ICSD data. Unlike most other solid-state coatings for the carbon layer, the carbon coating used in this study was relatively more uniform, although thick patches in some areas were observed. Furthermore, high crystallinity of all samples was further confirmed by the presence of a SAED pattern. In addition, the collapse of crystallinity in samples using Mn as TM was recorded from Na 1.1 (NMO-2) through to Na 1.3 (NMO-4) in Fig. S-10. As revealed in the XRD analysis, the Na 1.3 showed poor crystallinity through a ring formation along with bright spots. The structure may have started collapsing due to insufficient TM content and excessive Na ion accommodation on a layered structure, and is discussed further in later sections.

3.3. Electrochemical analysis

The electrodes were analyzed in half-cell mode by coupling with metallic Na as a counter electrode and were evaluated for suitability as cathode. Fig. 3 shows the galvanostatic charge–discharge (GCD) run between 1.5 and 4.0 V vs Na^+/Na for NMO samples and 2.0–3.6 V vs Na^+/Na for NCO samples. In both cases the charge-discharge profiles accurately reflect their respective CV. Additionally, the flat plateaus during charge/discharge were in match with the peak potentials of their respective CV. During the initial cycle, NMO-1.1 could deliver a high capacity of 197 mAh/g of sp. capacity at a current density of 10 mA/g. Increasing the current density further, the NMO-1.1 material could deliver values of 127, 104.8, 87.3, and 58.75 mAh/g of sp. capacity at current densities of 10, 25, 50, 100, and 500 mA/g. respectively, As seen in Fig. 4, during the initial cycle, NCO-1.05 could deliver the highest capacity of 124 mAh/g at a current density of 25 mA/g which is near

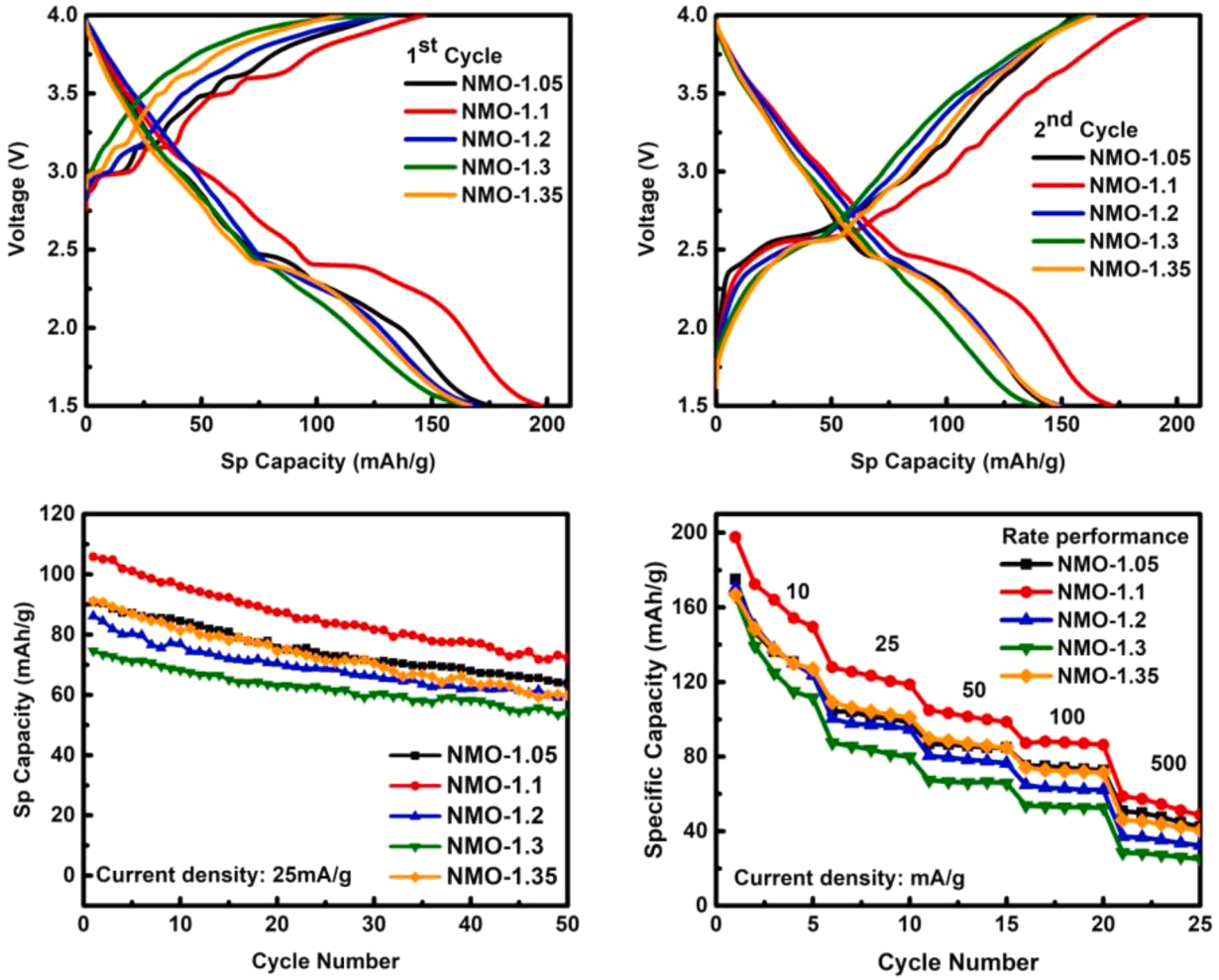

Fig. 3. GCD of 1st and 2nd cycle (A and B) for NMO materials with cycle stability (C) and rate performance (D).

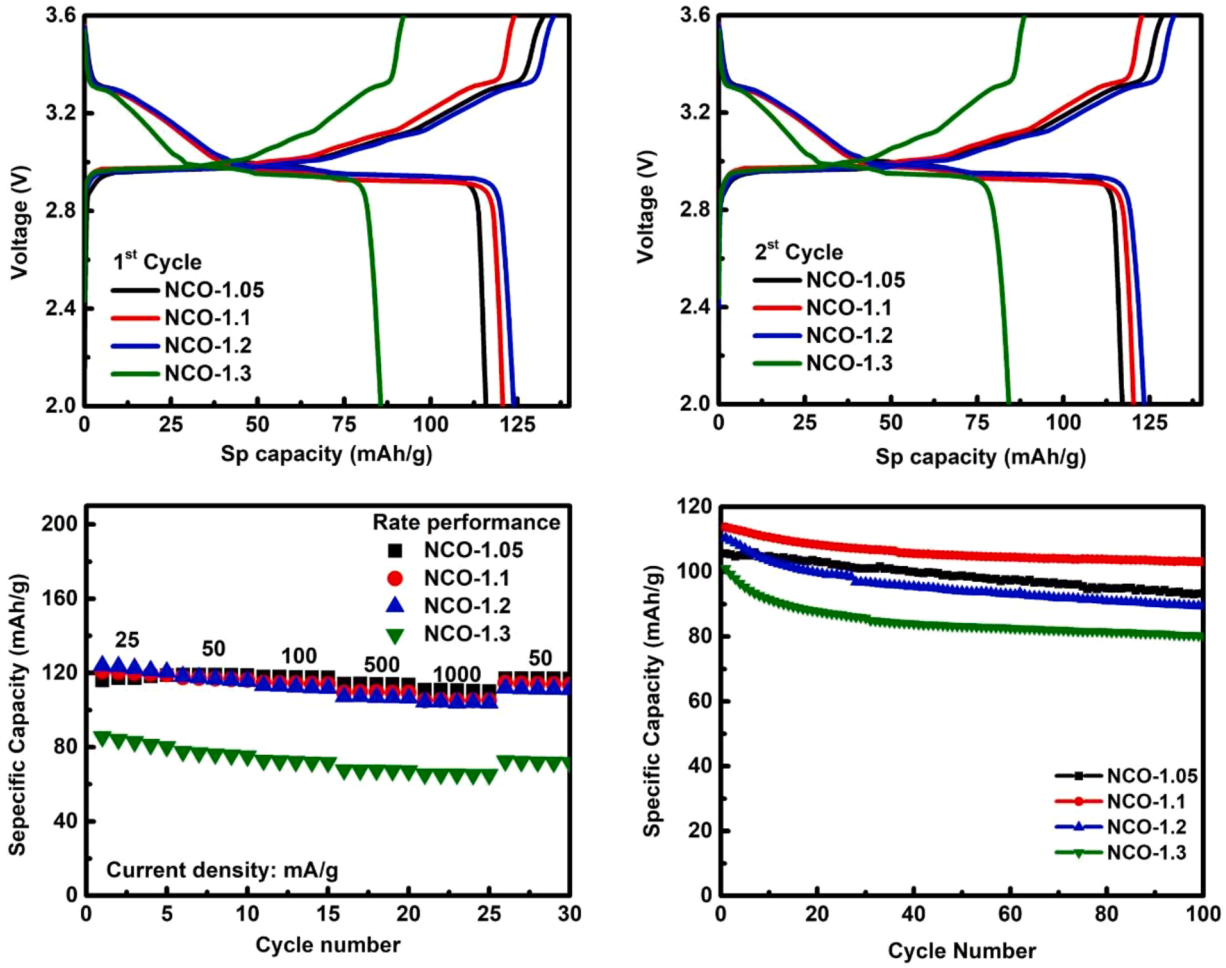

Fig. 4. GCD of 1st and 2nd cycle (A and B) for NCO materials with cycle stability (C) and rate performance (D).

equal to other stoichiometries too. Pushing the electrodes to higher current densities, Na-rich NCO-1.1 could deliver a much higher rate performance of 105 mAh/g of capacity at current densities of 25, 50, 100, and 500 mA/g, far better than the NMO materials. Though both transition metals used in this study are adjacent to each other on the periodic table, their behavior as a layered transition metal oxide and corresponding rate performances was drastically different. It was clear that ionic size and electronic configuration of this TM played a key role in determining or improving the capacity. To further show the effects of TM choice in long term stability, NCO materials could display a very high cycle stability of 90% or more over 100 cycles in all samples whereas the NMO could not display the same retention for even 50 cycles. This emphasized the fact that beyond doping in sites, coating, or adoption of other various strategies, choice of TM plays a crucial role in determining the basic performance standard. As the ionic size plays such a vital role, due to our increased Na stoichiometry and reduced TM content, the oxidation state of TM is highly affected. Based on following equation, the NCO and NMO cathodes undergo charging and discharging process.

$$NaTMO_2 \rightarrow TMO_2 + Na^+ + e^- \ (Charging)$$
$$TMO_2 + Na^+ + e^- \rightarrow NaTMO_2 \ (Discharging)$$

Where TM = Mn, Cr

During this charging process, it is well known that the oxidation state of TM ions changes from the +3 to the +4 state, during which the ionic size of the TM also changes. In the case of NCO samples, where Cr is used as TM, the ionic size is reduced from 0.615 to 0.55 Å [34,35], whereas in NMO samples where Mn is used as TM, the ionic size is reduced from 0.645 to 0.53 Å which is a significantly greater change than in the Cr case. Such a change in ionic size in every layer of the TM-O slab affects its thickness and overall structure which occurs every charge and discharge cycle. Translating this structural change to macroscale, such a change affects the structural integrity leading to a consistent loss of capacity for each cycle. When Na content was increased from 1.05 to 1.3 in particular, the capacity retention% of both NMO-1.1 and NCO-1.1 improved significantly. The increase in capacity retention can be due to modification of the oxidation state of the TM. This is because the local oxidation states of nearby TM atoms also change, leading to a big change in electron clouds. In macroscale, this small adjustment to the oxidation state of TM ions, which are structural backbones of the material, can result in improved stability overall.

Electrochemical analysis of all the samples was performed to determine a better working window of cathode materials. Additionally, CV at low scan rates can give insight into the mechanisms of the charge and discharge process. As shown in Fig. 5, for NMO samples, the potential window is initially chosen between 1.5 and 4.0 V vs Na/Na^+. Realizing the stability and reversibility of both electrode and electrolyte in the given window, the potential(E) window was further pushed to a higher potential of 4.2 V to achieve high energy density (Fig. S-1). Initial analysis suggested that NMO materials display sharp redox peaks with high intensity implying faster kinetics of the charge/discharge process with high reversibility. Minor peaks at E greater than 2.5 V and a major peak at approximately 2.3 V (during cathodic sweep) and 2.6 V (during anodic sweep) can be seen reflected as flat plateaus in discharge and charge GCD as well. As earlier reported by Sato et al. [36]., $NaMnO_2$ undergoes charge/discharge process in a complicated and multiple phase transitions happening during cycling. Also it may be associated

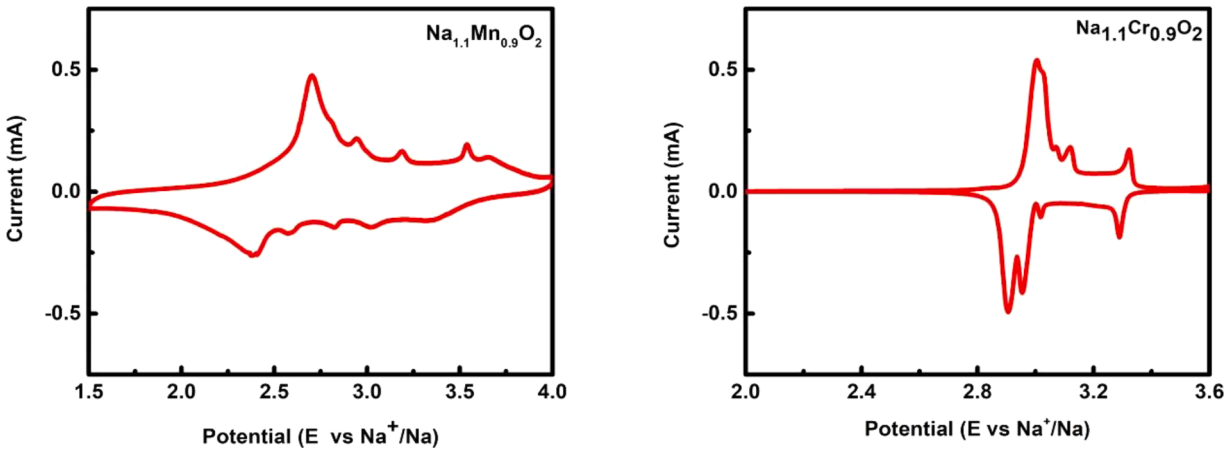

Fig. 5. Cyclic voltammogram of Na-rich cathode material NMO (left) and NCO (right).

with charge, spin and orbital ordering on desodiation. Hence a subtle multiphase transition is happening leading to near smooth GCD curves. These major peak E can be attributed to the point at which major Na intercalation or decalation takes place. With this in mind, the electrode was further pushed to 4.2 V at which the major peak (when normalised for mass loading) intensities were significantly reduced due to reduced intercalation or decalation process resulting in reduced capacity. Though 5 cycles are insufficient to fully understand the stability of cathode, the peak remained firm at a particular E with little loss in intensity. This can be loosely translated to superior structural stability of the material.

3.4. Na ion diffusion analysis

Further CV were recorded at different scan rates to analyze the diffusion coefficient D_0 of the Na^+ electrode-electrolyte interface using the Randles–Sevcik equation. For the NMO samples, the CV were detected between 1.5 and 4.0 V and the peak currents were recorded for each scan rate as shown in Fig. S-2. The obtained peak currents were then solved using following equation:

$i_p = kn^{3/2}AD_o^{1/2}v^{1/2}C_{Na+}$, where i_p (A) is the peak current in the given scan rate, k is a constant with value of 2.69×10^5 (A s mol^{-1} $V^{-1/2}$) under standard condition of 25ºC. The other parameters such as number of electrons involved n, scan rate ν (V s^{-1}), concentration of oxidized species C_O*, sodium ion concentration C_{Na+} (in mol cm^{-3}) and electrode area A (cm^2) are determined experimentally and specific to each setup and the material properties. Since the Randles equation is based on the assumption that ion diffusion through liquid medium is not complicated by any migration, the equation tends to fail in solid medium as the diffusion mechanisms are more complicated [37]. Thus, it is necessary to clarify that, many recently published articles that also report on Na ion diffusion using cell parameter data for Na ion concentration and BET surface analysis for electrode surfaces, which is incorrect or invalid as per the aforementioned point. Therefore, we use concentration of electrolyte here to determine the sodium ion diffusion in electrolyte-electrode interface otherwise known as the SEI layer. Using this SEI layer, the diffusivity of the Na^+ ion was determined to be 1.91×10^{-8} cm^2 s^{-1} for the NMO-2 sample and 2.73×10^{-9} cm^2 s^{-1} for the NCO-2 sample. On comparison, the NMO and NCO materials display a higher order of diffusivity than many earlier reported samples. This higher diffusivity can be attributed to superior performance and a better SEI layer that facilitates faster intercalation kinetics.

3.5. Rietveld- refinement analysis

To better understand the change in crystal structure with increase in sodium stoichiometry, Rietveld analyses were performed for all NCO samples using Profex software [38]. Understanding the cell parameters and electron density mapping gives better insight into the NCO samples at an atomic level. After systematic Rietveld analysis, the cell parameters of various NCO materials were tabulated in Table 1. Unlike in various other cases [11,12] where NCO cathodes were refined with the R3m space group of rhombohedral crystal structure, this system was refined with the P1 space group corresponding to triclinic structures where $a \neq b \neq c$ and $\alpha \neq \beta \neq \gamma$. Since all of the previous reports are made on sodium deficient (Na < 0.95) NCO cathodes, the structure was rhombohedral (R3m) in nature with $a = b \neq c$ and $\alpha = \beta = 90^o$, $\gamma = 120^o$. Due to accommodation of excess sodium the structure undergoes a slight change in Tm binding energy Table S-2 as well as crystal parameters resulting in a triclinic (P1) crystal structure. Though the cell parameter values are not much different from those of the R3m space group, the change in lattice parameters leads a disruption in the crystal lattice. Such disruption causes a capacity increase in this sodium rich cathode. Fig. S-7 displays the change in values of c and γ of NCO unit cell. In order to find where the excess sodium is located, possible sodium rich phases or compounds were investigated. It was found that other than NCO, two more Na–rich phases, Na_2CrO_7 and Na_2CO_3, were also present, and their presence increased significantly with an increase in Na stoichiometry. As shown in Fig. S-8, with each increase in sodium stoichiometry, a proportionate increase in Na_2CO_3 was observed, which likely resulted in equivalent capacity loss in Na 1.2 and Na 1.3 cathodes.

3.6. Electron density map analysis

Electron density mapping is a common analysis technique used in biochemistry to analyze the electron cloud behavior around a particular atom or set of atoms in a unit cell. It is seldom used for studying Li ion [32,39] and Mg ion battery [40] electrode materials. However, this electron cloud behavior analysis can be exploited to find the nature of a bond among atoms in a crystal structure, such as whether it is ionic or covalent. To understand the electron cloud behavior and changes in bond nature in the sample sodium-rich cathodes, X-ray diffraction data were used, and the refinement data electron density map is plotted in Fig. 6 using Profex software [38]. In the map, distinct changes in the electron cloud and the bonding between Na-O and Cr-O with each increase in sodium ion stoichiometry are observed. In most sodium ion cathodes, oxygen loss is the key reason behind capacity fading and also causes various safety concerns. To study the same with electron density, in the case of Na 1.05, the electron clouds were found equally scattered throughout. The electron density maxima and minima were very close to the O and Cr atoms respectively suggesting a relatively weaker bond between them. With a slight increase in Na concentration to Na 1.1, an ionic-type bonding was observed between Cr and O, shown by electron

Table 1
Calculated cell parameter data using Rietveld refinement.

Sodium stoichiometry	Cell parameters						R_{wp}	R_{exp}	χ^2	GOF
	a (nm)	b (nm)	c (nm)	α	β	γ				
1.05	0.298 (±0.001)	0.298 (±0.0003)	1.600 (±0.0008)	90.040 (±0.1)	89.930 (±0.2)	120.095 (±0.09)	1.170	1.090	1.152	1.073
1.1	0.298 (±0.002)	0.298 (±0.001)	1.597 (±0.001)	90.140 (±0.01)	89.912 (±0.009)	120.690 (±0.007)	2.780	2.670	1.084	1.041
1.2	0.299 (±0.001)	0.300 (±0.001)	1.597 (±0.01)	90.072 (±0.01)	90.029 (±0.01)	120.702 (±0.008)	2.860	2.720	1.106	1.051
1.3	0.298 (±0.0002)	0.300 (±0.002)	1.596 (±0.0002)	89.873 (±0.3)	90.054 (±0.6)	120.042 (±0.8)	2.940	2.780	1.118	1.058

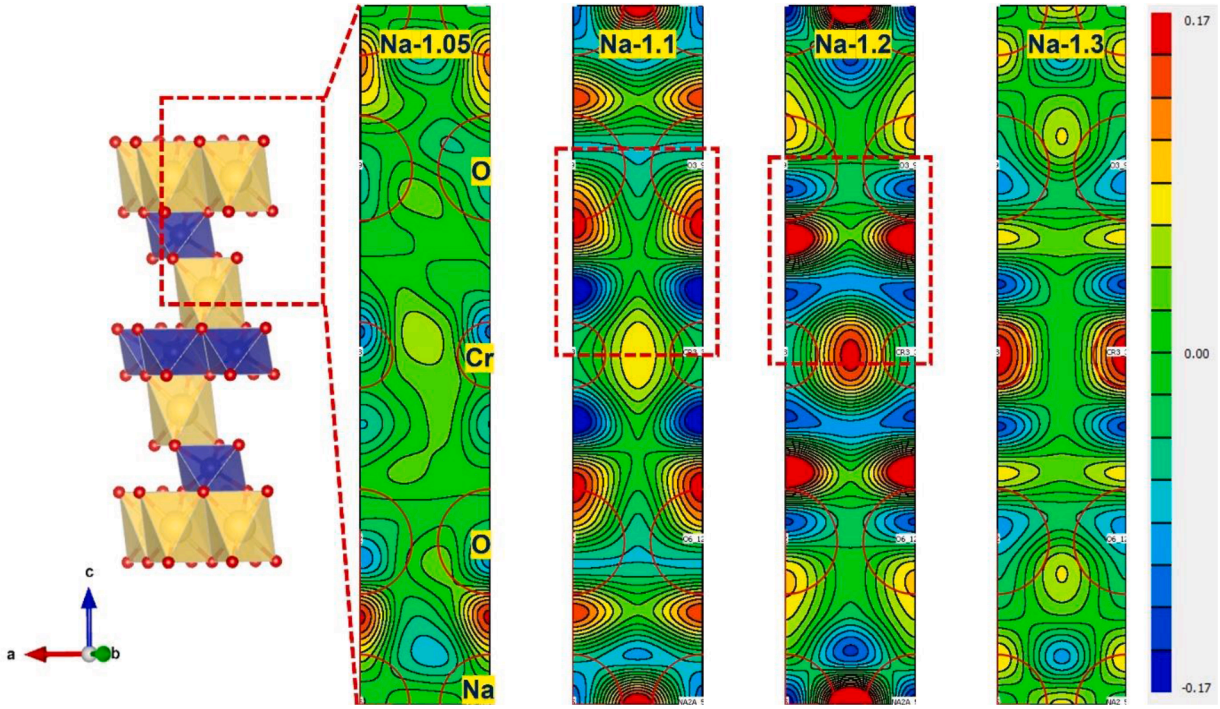

Fig. 6. Electron density map for NCO cathode predicted using refinement data. Strong ionic type bond between Cr and O is highlighted by red box.

density maxima (red) and minima (blue) both appearing in between Cr and O atoms. Such ionic-type bonding leads to the improved stability of the Cr-O bond resulting in overall electrochemical stability. A similar trend was observed in Na 1.2 and Na 1.3 but at a reduced intensity, implying relatively weaker bonding. $Na_{1.1}Cr_{0.9}O_2$ displayed the best performance in terms of both capacity and cycle stability.

3.7. Full-cell analysis

To better understand the cathode materials for practical application, the cathodes were coupled with hard carbon anodes. For better SEI layer formation and superior performance, the hard carbon was presodiated by coupling with Na metal and used after 3 charge-discharge cycles. To represent both NMO and NCO cases, their best samples were used as cathode and hard carbon as anode in Fig. 7. The cells were cycled between 1.2 and 3.7 V at various current densities for analyzing its rate performance. In full cell configuration the NMO cathode could deliver a maximum energy density of 200 Wh Kg^{-1} and a maximum power density of 625 KW Kg^{-1} for energy density more than 80 Wh kg^{-1}. In comparison, the NCO-based full cell could deliver a maximum energy density of 220 Wh Kg^{-1} and a maximum density of 1100 W Kg^{-1}, likely due to superior performance in half cell and stability, as shown in Fig. S-4. Although almost identical synthesis techniques and the same Na ion stoichiometry were used, a seemingly small change in TMs that are next to each other on the periodic table could drastically change the overall behavior of this entire battery system both in terms of rate performance and stability. This study also clearly elucidates the impact of an increase in Na content and its effect on the TM, in turn affecting the overall performance. It is understood that a DFT study could give better insight into this system, and a further study is planned accordingly. Overall, it has been found that NCO materials display better properties than NMO materials and has an advantage due to their electronic configuration (Table 2).

4. Conclusion

Na-rich cathode materials with Mn and Cr as a transition metal were synthesized using simple solid-state techniques, and their electrochemical and phase behaviors were analyzed. Compared with its Mn counterpart, the Cr-based Na-rich cathode performed better in every aspect, such as half-cell performance, rate performance, cycle stability, and initial charge discharge. XRD showed that this superior performance could be attributed to the better structural stability of the Cr-based cathode than the Mn-based cathode. Although an increase in the sodium stoichiometry should theoretically increase capacity, the formation of a spinel phase in the case of NMO materials and an impure Na_2CO_3 phase in NCO materials led to a capacity drop. Finally, a CR2032 coin cell was constructed using hard carbon as an anode, and it

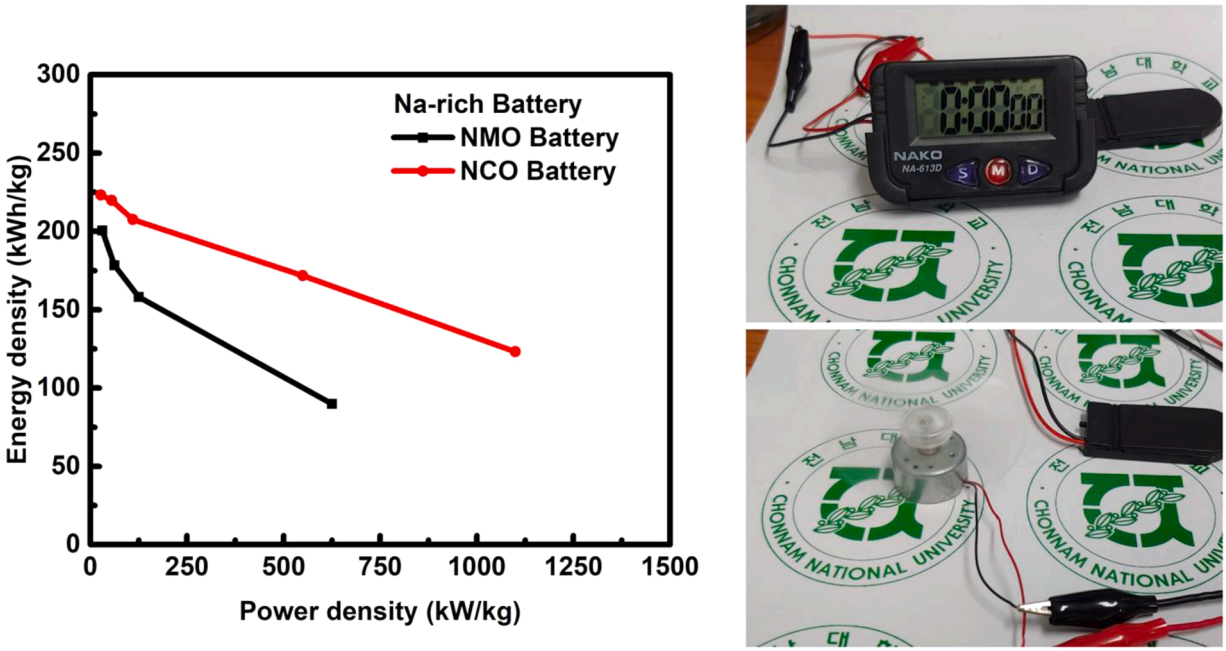

Fig. 7. Ragone plot for Na-ion battery using different Na-rich cathode material and hard carbon anode.

Table 2
Comparison of the rate capability and performance in this study with those in previous reports.

Electrode material	Current density	C- rate	Capacity (mAh/g)	Group	Cathode type
$Na_{1.1}Cr_{0.9}O2$	1000		105	Our Work	Layered cathode material
Prussian blue material	1000		20	Wang et al. [41]	PB type
Highly crystalline nickel hexacyanoferrate	850		50	Rehman et al. [42]	PB type
Fe substitution for Ru in disordered Na1.33Ru0.67O2		2	61	Siriwardena et al. [7]	Layered cathode material
$Na_{0.86}Ti_{0.73}[Fe(CN)_6]\bullet 3H_2O)$		0.05	74	Giorgetti et al. [43]	PB type
Prussian white ($Na_{3.1}Fe_4[Fe(CN)_6]_3$) hierarchical nanotubes		50	83	Ren et al. [44]	PB type
$Na_xMnFe(CN)_6$		10	86.6	Shen et al. [45]	PB type
$Na_xMn[Fe(CN)_6]y$	750		109.2	Fu et al. [46]	PB type
$P2\text{-}Li_{0.2}Na_{1.0}Mn_{0.8}O_2$	50		120	Zhu et al. [47]	Layered cathode material
Sodium manganese hexacyanoferrate (Mn-HCF)	12	0.1	128	Li et al. [48]	PB type
$Na_{1.58}Fe[Fe(CN)_6]_{0.92}$		0.1	142	Tang et al. [49]	PB type
$Na_4V_2O_7$	10		160	Su et al. [50]	Layered cathode material
$Na_{1.2}Mn_{0.4}Ir_{0.4}O_2$		0.1	179	Zhang et al. [28]	Layered cathode material

exhibited a cycle stability of higher than 83% after 100 cycles. Furthermore, a working setup was created using a single cell to better display its performance. Based on the approaches employed in this current study, it is clear that rather than doping a layered structure with complex atoms for improving capacity and various other performance metrics, increasing Na stoichiometry can improve the same characteristics and open a new avenue of Na-rich cathode materials.

CRediT authorship contribution statement

Bala Krishnan Ganesan: Conceptualization, Methodology, Formal analysis, Investigation, Software, Visualization, Writing – original draft. **Ui Rim Son:** Conceptualization, Methodology, Formal analysis, Investigation, Writing – original draft. **Ranjith Thangavel:** Methodology, Formal analysis, Investigation, Visualization, Writing – review & editing. **Yun-Sung Lee:** Funding acquisition, Resources, Supervision, Visualization, Validation, Writing – review & editing.

Declaration of Competing Interest

The authors declare that they have no known competing financial interests or personal relationships that could have appeared to influence the work reported in this paper.

Acknowledgement

This work was supported by the National Research Foundation of Korea (NRF) grant funded by the Korean government (Ministry of Science, ICT & Future Planning) (No. 2019R1A2C1007620). Dr. Ranjith Thangavel acknowledges the support from IIT Guwahati through the Stratup Research grant. BK would like to thank Dr Kalpana Dharmalingam, CECRI, Chennai Unit for her valuable discussions.

Supplementary materials

Supplementary material associated with this article can be found, in the online version, at doi:10.1016/j.electacta.2022.140493.

References

[1] R. Thangavel, M. Moorthy, B.K. Ganesan, W. Lee, W. Yoon, Y. Lee, Nanoengineered organic electrodes for highly durable and ultrafast cycling of organic sodium-ion batteries, Small 16 (2020), 2003688, https://doi.org/10.1002/smll.202003688.
[2] M. Wu, W. Ni, J. Hu, J. Ma, NASICON-structured $NaTi_2(PO_4)_3$ for sustainable energy storage, Nano Micro Lett. 11 (2019) 1–36, https://doi.org/10.1007/s40820-019-0273-1.
[3] F. Hu, S. Liu, S. Li, C. Liu, G. Yu, C. Song, W. Shao, T. Zhang, X. Jian, High and ultra-stable energy storage from all-carbon sodium-ion capacitor with 3D

framework carbon as cathode and carbon nanosheet as anode, J. Energy Chem. 55 (2021) 304–312, https://doi.org/10.1016/j.jechem.2020.06.034.
[4] H. Li, X. Zhang, Z. Zhao, Z. Hu, X. Liu, G. Yu, Flexible sodium-ion based energy storage devices: recent progress and challenges, Energy Storage Mater. 26 (2020) 83–104, https://doi.org/10.1016/j.ensm.2019.12.037.
[5] H.V. Ramasamy, K. Kaliyappan, R. Thangavel, W.M. Seong, K. Kang, Z. Chen, Y. S. Lee, Efficient method of designing stable layered cathode material for sodium ion batteries using aluminum doping, J. Phys. Chem. Lett. 8 (2017) 5021–5030, https://doi.org/10.1021/acs.jpclett.7b02012.
[6] H.V. Ramasamy, K. Kaliyappan, R. Thangavel, V. Aravindan, K. Kang, D.U. Kim, Y. Park, X. Sun, Y.S. Lee, Cu-doped P2-$Na_{0.5}Ni_{0.33}Mn_{0.67}O_2$ encapsulated with MgO as a novel high voltage cathode with enhanced Na-storage properties, J. Mater. Chem. A. 5 (2017) 8408–8415, https://doi.org/10.1039/c6ta10334k.
[7] D.P. Siriwardena, J.F.S. Fernando, T. Wang, K.L. Firestein, C. Zhang, J.E. von Treifeldt, D.V. Golberg, Effect of Fe^{3+} for Ru^{4+} substitution in disordered $Na_{1.33}Ru_{0.67}O_2$ cathode for sodium-ion batteries: structural and electrochemical characterizations, Electrochim. Acta 325 (2019), 134926, https://doi.org/10.1016/j.electacta.2019.134926.
[8] Y. Zhu, W. Nie, P. Chen, Y. Zhou, Y. Xu, Li-doping stabilized P2-$Li_{0.2}Na_{1.0}Mn_{0.8}O_2$ sodium ion cathode with oxygen redox activity, Int. J. Energy Res. 44 (2020) 3253–3259, https://doi.org/10.1002/er.5120.
[9] J. Duan, G. Qin, L. Min, Y. Yang, C. Wang, Ultraviolet irradiation treatment for enhanced sodium storage performance based on wide-interlayer-spacing hollow C@MoS_2@CN nanospheres, ACS Appl. Mater. Interfaces 10 (2018) 38084–38092, https://doi.org/10.1021/acsami.8b13570.
[10] C. Wang, L. Liu, S. Zhao, Y. Liu, Y. Yang, H. Yu, S. Lee, G.H. Lee, Y.M. Kang, R. Liu, F. Li, J. Chen, Tuning local chemistry of P2 layered-oxide cathode for high energy and long cycles of sodium-ion battery, Nat. Commun. 12 (2021) (2021) 1–9, https://doi.org/10.1038/s41467-021-22523-3.
[11] I. Lee, G. Oh, S. Lee, T.Y. Yu, M.H. Alfaruqi, V. Mathew, B. Sambandam, Y.K. Sun, J.Y. Hwang, J. Kim, Cationic and transition metal co-substitution strategy of O_3-type $NaCrO_2$ cathode for high-energy sodium-ion batteries, Energy Storage Mater. 41 (2021) 183–195, https://doi.org/10.1016/J.ENSM.2021.05.046.
[12] C.-.Y. Yu, J.-.S. Park, H.-.G. Jung, K.-.Y. Chung, D. Aurbach, Y.K. Sun, S.T. Myung, $NaCrO_2$ cathode for high-rate sodium-ion batteries, Energy Environ. Sci. 8 (2015) 2019–2026, https://doi.org/10.1039/C5EE00695C.
[13] S. Guo, Y. Sun, J. Yi, K. Zhu, P. Liu, Y. Zhu, G.Z. Zhu, M. Chen, M. Ishida, H. Zhou, Understanding sodium-ion diffusion in layered P2 and P3 oxides via experiments and first-principles calculations: a bridge between crystal structure and electrochemical performance, NPG Asia Mater. 84 (2016) (2016) e266, https://doi.org/10.1038/am.2016.53.
[14] C. Delmas, C. Fouassier, P. Hagenmuller, Structural classification and properties of the layered oxides, Phys. B+C 99 (1980) 81–85, https://doi.org/10.1016/0378-4363(80)90214-4.
[15] S. Komaba, C. Takei, T. Nakayama, A. Ogata, N. Yabuuchi, Electrochemical intercalation activity of layered $NaCrO_2$ vs. $LiCrO_2$, Electrochem. Commun. 12 (2010) 355–358, https://doi.org/10.1016/J.ELECOM.2009.12.033.
[16] C. Didier, M. Guignard, C. Denage, O. Szajwaj, S. Ito, I. Saadoune, J. Darriet, C. Delmas, Electrochemical Na-deintercalation from $NaVO_2$, Electrochem. Solid-State Lett. 14 (2011), https://doi.org/10.1149/1.3555102.
[17] R. Berthelot, D. Carlier, C. Delmas, Electrochemical investigation of the P2-Na_xCoO_2 phase diagram, Nat. Mater. 10 (2011) 74–80, https://doi.org/10.1038/NMAT2920.
[18] X. Yan, Y. Yang, E. Liu, L. Sun, H. Wang, X.Z. Liao, Y. He, Z.F. Ma, Improved cycling performance of prussian blue cathode for sodium ion batteries by controlling operation voltage range, Electrochim. Acta 225 (2017) 235–242, https://doi.org/10.1016/j.electacta.2016.12.121.
[19] Y. You, X. Yu, Y. Yin, K.W. Nam, Y.G. Guo, Sodium iron hexacyanoferrate with high Na content as a Na-rich cathode material for Na-ion batteries, Nano Res. 8 (2014) 117–128, https://doi.org/10.1007/s12274-014-0588-7.
[20] J. Qian, C. Wu, Y. Cao, Z. Ma, Y. Huang, X. Ai, H. Yang, Prussian blue cathode materials for sodium-ion batteries and other ion batteries, Adv. Energy Mater. 8 (2018), 1702619, https://doi.org/10.1002/aenm.201702619.
[21] M. Xie, M. Xu, Y. Huang, R. Chen, X. Zhang, L. Li, F. Wu, $Na_2Ni_xCo_{1-x}Fe(CN)_6$: a class of Prussian blue analogs with transition metal elements as cathode materials for sodium ion batteries, Electrochem. Commun. 59 (2015) 91–94, https://doi.org/10.1016/j.elecom.2015.07.014.
[22] Z. Shen, S. Guo, C. Liu, Y. Sun, Z. Chen, J. Tu, S. Liu, J. Cheng, J. Xie, G. Cao, X. Zhao, Na-rich prussian white cathodes for long-life sodium-ion batteries, ACS Sustain. Chem. Eng. 6 (2018) 16121–16129, https://doi.org/10.1021/acssuschemeng.8b02758.
[23] J. Luo, S. Sun, J. Peng, B. Liu, Y. Huang, K. Wang, Q. Zhang, Y. Li, Y. Jin, Y. Liu, Y. Qiu, Q. Li, J. Han, Y. Huang, Graphene-roll-wrapped prussian blue nanospheres as a high-performance binder-free cathode for sodium-ion batteries, ACS Appl. Mater. Interfaces 9 (2017) 25317–25322, https://doi.org/10.1021/acsami.7b06334.
[24] W. Ren, Z. Zhu, M. Qin, S. Chen, X. Yao, Q. Li, X. Xu, Q. Wei, L. Mai, C. Zhao, Prussian white hierarchical nanotubes with surface-controlled charge storage for sodium-ion batteries, Adv. Funct. Mater. 29 (2019), 1806405, https://doi.org/10.1002/adfm.201806405.
[25] J.P. Baboo, J. Song, S. Kim, J. Jo, S. Baek, V. Mathew, D.T. Pham, M.H. Alfaruqi, Z. Xiu, Y.K. Sun, J. Kim, Monoclinic-Orthorhombic $Na_{1.1}Li_{2.0}V_2(PO_4)_3$/C Composite Cathode for Na+/Li+ Hybrid-Ion Batteries, Chem. Mater. 29 (2017) 6642–6652, https://doi.org/10.1021/acs.chemmater.7b00856.
[26] N.V. Kosova, D.O. Rezepova, S.A. Petrov, A.B. Slobodyuk, Electrochemical and chemical Na + /Li + ion exchange in na-based cathode materials: $Na_{1.56}Fe_{1.22}P_2O_7$ and $Na_3V_2(PO_4)_2F_3$, J. Electrochem. Soc. 164 (2017) A6192–A6200, https://doi.org/10.1149/2.0301701jes.
[27] N. Su, Y. Lyu, B. Guo, Electrochemical and *in-situ* X-ray diffraction studies of $Na_{1.2}Ni_{0.2}Mn_{0.2}Ru_{0.4}O_2$ as a cathode material for sodium-ion batteries, Electrochem. Commun. 87 (2018) 71–75, https://doi.org/10.1016/j.elecom.2017.12.029.
[28] X. Zhang, Y. Qiao, S. Guo, K. Jiang, S. Xu, H. Xu, P. Wang, P. He, H. Zhou, Manganese-based Na-rich materials boost anionic redox in high-performance layered cathodes for sodium-ion batteries, Adv. Mater. 31 (2019), 1807770, https://doi.org/10.1002/adma.201807770.
[29] Z. Lun, B. Ouyang, R.J. Clément, D.H. Kwon, G. Ceder, High-capacity Mn-based cation-disordered rocksalt cathodes, ECS Meet. Abstr. (2020) 187, https://doi.org/10.1149/ma2020-012187mtgabs.
[30] M. Armand, J. Tarascon, Building better batteries我的大论文 Josephson, Nature 451 (2008) 2–7.
[31] C. Zhao, Q. Wang, Z. Yao, J. Wang, B. Sánchez-Lengeling, F. Ding, X. Qi, Y. Lu, X. Bai, B. Li, H. Li, A. Aspuru-Guzik, X. Huang, C. Delmas, M. Wagemaker, L. Chen, Y.S. Hu, Rational design of layered oxide materials for sodium-ion batteries, Science 370 (80) (2020) 708–712, https://doi.org/10.1126/SCIENCE.AAY9972/FORMAT/PDF.
[32] Mechanical and structural degradation of LiNixMnyCozO2 cathode in Li-ion batteries: an experimental study, (2017). 10.1149/2.1751713jes.
[33] L. Zheng, H. Wang, M. Luo, G. Wang, Z. Wang, C. Ouyang, Na_2MnO_3 as cathode materials for Na ion batteries: from first-principles investigations, Solid State Ion. 320 (2018) 210–214, https://doi.org/10.1016/J.SSI.2018.02.039.
[34] Q. Liu, Z. Hu, W. Li, C. Zou, H. Jin, S. Wang, S. Chou, S.X. Dou, Sodium transition metal oxides: the preferred cathode choice for future sodium-ion batteries? Energy Environ. Sci. 14 (2021) 158–179, https://doi.org/10.1039/D0EE02997A.
[35] R.D. Shannon, Revised effective ionic radii and systematic studies of interatomic distances in halides and chalcogenides, Acta Crystallogr. Sect. A 32 (1976) 751–767, https://doi.org/10.1107/S0567739476001551.
[36] T. Sato, K. Yoshikawa, W. Zhao, T. Kobayashi, H.B. Rajendra, M. Yonemura, N. Yabuuchi, Efficient stabilization of Na storage reversibility by Ti integration into O ′ 3-type NaMnO2, (2021). 10.34133/2021/9857563.
[37] B.J. E B Randles, go-a Erdey Gruz and Volmer, 2. physzk. Chem, 1938.
[38] N. Doebelin, R. Kleeberg, Profex: a graphical user interface for the Rietveld refinement program BGMN, J. Appl. Crystallogr. 48 (2015) 1573–1580, https://doi.org/10.1107/S1600576715014685.
[39] Z. Jiang, J. Li, Y. Yang, L. Mu, C. Wei, X. Yu, P. Pianetta, K. Zhao, P. Cloetens, F. Lin, Y. Liu, Machine-learning-revealed statistics of the particle-carbon/binder detachment in lithium-ion battery cathodes, Nat. Commun. 111 (11) (2020) 1–9, https://doi.org/10.1038/s41467-020-16233-5.
[40] M.S. Chae, J. Hyoung, M. Jang, H. Lee, S.T. Hong, Potassium nickel hexacyanoferrate as a high-voltage cathode material for nonaqueous magnesium-ion batteries, J. Power Sources 363 (2017) 269–276, https://doi.org/10.1016/J.JPOWSOUR.2017.07.094.
[41] W. Wang, Y. Gang, Z. Hu, Z. Yan, W. Li, Y. Li, Q.F. Gu, Z. Wang, S.L. Chou, H.K. Liu, S.X. Dou, Reversible structural evolution of sodium-rich rhombohedral Prussian blue for sodium-ion batteries, Nat. Commun. 111 (2020) (2020) 1–9, https://doi.org/10.1038/s41467-020-14444-4.
[42] R. Rehman, J. Peng, H. Yi, Y. Shen, J. Yin, C. Li, C. Fang, Q. Li, J. Han, Highly crystalline nickel hexacyanoferrate as a long-life cathode material for sodium-ion batteries, RSC Adv. 10 (2020) 27033–27041, https://doi.org/10.1039/D0RA03490H.
[43] M. Li, A. Mullaliu, S. Passerini, M. Giorgetti, Titanium activation in prussian blue based electrodes for Na-ion batteries: a synthesis and electrochemical study, Batteries 7 (2021) (2021) 5, https://doi.org/10.3390/BATTERIES7010005.
[44] W. Ren, Z. Zhu, M. Qin, S. Chen, X. Yao, Q. Li, X. Xu, Q. Wei, L. Mai, C. Zhao, Prussian white hierarchical nanotubes with surface-controlled charge storage for sodium-ion batteries, Adv. Funct. Mater. 29 (2019), 1806405, https://doi.org/10.1002/ADFM.201806405.
[45] Z. Shen, S. Guo, C. Liu, Y. Sun, Z. Chen, J. Tu, S. Liu, J. Cheng, J. Xie, G. Cao, X. Zhao, Na-Rich prussian white cathodes for long-life sodium-ion batteries, ACS Sustain. Chem. Eng. 6 (2018) 16121–16129, https://doi.org/10.1021/ACSSUSCHEMENG.8B02758.
[46] H. Fu, M. Xia, R. Qi, X. Liang, M. Zhao, Z. Zhang, X. Lu, G. Cao, Improved rate performance of Prussian blue cathode materials for sodium ion batteries induced by ion-conductive solid-electrolyte interphase layer, J. Power Sources. 399 (2018) 42–48, https://doi.org/10.1016/j.jpowsour.2018.07.071.
[47] Y. Xi, Y. Lu, Rapid synthesis of sodium-rich Prussian white for sodium-ion battery via a bottom-up approach, Chem. Eng. J. 405 (2021), 126688, https://doi.org/10.1016/J.CEJ.2020.126688.
[48] Y. Zhu, W. Nie, P. Chen, Y. Zhou, Y. Xu, Li-doping stabilized P2-$Li_{0.2}Na_{1.0}Mn_{0.8}O_2$ sodium ion cathode with oxygen redox activity, Int. J. Energy Res. 44 (2020) 3253–3259, https://doi.org/10.1002/ER.5120.
[49] X. Tang, H. Liu, D. Su, P.H.L. Notten, G. Wang, Hierarchical sodium-rich Prussian blue hollow nanospheres as high-performance cathode for sodium-ion batteries, Nano Res. 118 (2018) 3979–3990, https://doi.org/10.1007/S12274-018-1979-Y.
[50] B. Su, H. Liang, J. Liu, J. Wu, N. Sharma, Q. Gu, B. Johannessen, D.Y.W. Yu, Novel structurally-stable Na-rich $Na_4V_2O_7$cathode material with high reversible capacity by utilization of anion redox activity, Chem. Commun. 56 (2020) 8245–8248, https://doi.org/10.1039/d0cc02816a.